Science of the Total Environment 951 (2024) 175320

Contents lists available at ScienceDirect

Science of the Total Environment

journal homepage: www.elsevier.com/locate/scitotenv

Combination of biotransformation and metabolomics reveals tolfenpyrad-induced hepatocytotoxicity

Xin Jiang [1], Yingjie Zhu [1], Suhe Dong, Runfeng Lin, Peihong Zhu, Jie Mao, Yanqing Cao, Xiaoyao Yin, Fangting Dong, Kun He [*], Na Wang [*]

National Center of Biomedical Analysis, Beijing 100039, China

HIGHLIGHTS

- Toxicity mechanism of tolfenpyrad deciphered by biotransformation and metabolomics.
- Fourteen phase I and four phase II biotransformed products were characterized.
- Tolfenpyrad at environmental levels disturbs purine and glutathione metabolism.
- Hepatocytotoxicity of PT-CA is non-negligible in environmental risk assessments.

GRAPHICAL ABSTRACT

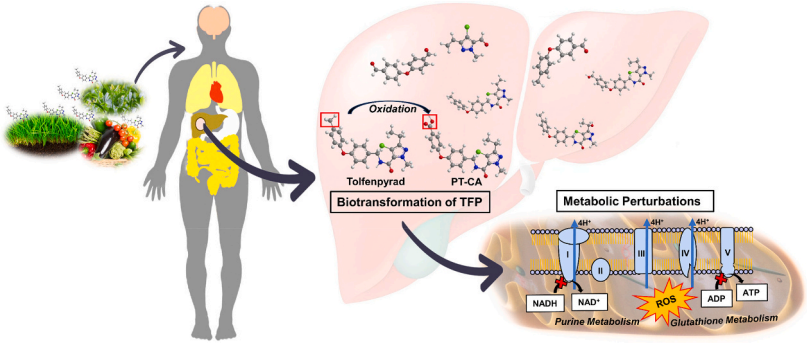

ARTICLE INFO

Editor: Henner Hollert

Keywords:
Risk assessment
Human liver microsome
Metabolism
Cytotoxicity
Mitochondria damage

ABSTRACT

Tolfenpyrad (TFP) is an extensively used pesticide that inevitably leads to human exposure to both TFP and its transformation product residues. However, the biotransformation of TFP in humans has not been elucidated, and the toxicity of TFP along with its biotransformation products remains largely unknown. In this study, the biotransformation process of TFP was investigated using human liver microsomes and human hepatic cells. Endogenous metabolic changes in the cells were studied to investigate the hepatocytotoxicity of TFP at environmentally relevant concentrations. Fourteen phase I biotransformation products and four phase II TFP products were characterized, among which twelve products were identified for the first time. The oxidative product tolfenpyrad-benzoic acid (PT-CA) was particularly abundant and stable. Further hepatotoxicity assessments and metabolic studies demonstrated comparable metabolic profiles for TFP and PT-CA in HepG2 cells, with both significantly disrupting purine and glutathione metabolism. These processes are closely associated with oxidative

Abbreviations: CYP, cytochrome P450; DILI, drug induced liver injury; DMSO, dimethyl sulfoxide; FMO, flavin monooxygenase; H_2O_2, hydrogen peroxide; H-HT, human hepatotoxicity; HLM, human liver microsomes; HRMS, high-resolution mass spectrometry; PBS, phosphate-buffered saline; PLS-DA, partial least squares discriminant analysis; PT-CA, tolfenpyrad-benzoic acid; OH-PT-CA, 4-[4-[[4-chloro-3-(1-hydroxyethyl) -1-methylpyrazol-5-yl]carbonylamino-methyl]phenoxy] benzoic acid; OH-PT, 4-chloro-3-(1-hydroxyethyl)-1-methyl-N-[4-(p-tolyloxy)benzyl] pyrazole-5-carboxamide; QTOF MS, quadrupole time-of-flight mass spectrometer; ROS, reactive oxygen species; TFP, tolfenpyrad; UHPLC, ultra-high-performance liquid chromatography; VIP, variable importance in the projection value; XO, xanthine oxidase.

* Corresponding authors at: National Center of Biomedical Analysis, Beijing, China.
E-mail addresses: hk@proteomics.cn (K. He), nwang@ncba.ac.cn (N. Wang).

[1] These authors contributed equally.

https://doi.org/10.1016/j.scitotenv.2024.175320
Received 15 April 2024; Received in revised form 10 June 2024; Accepted 4 August 2024
Available online 5 August 2024
0048-9697/© 2024 Elsevier B.V. All rights are reserved, including those for text and data mining, AI training, and similar technologies.

stress, mitochondrial damage, and cell death. Our results provide novel perspectives on the biotransformation, metabolism, and hepatotoxicity of TFP, thereby highlighting the non-negligible toxicity of its crucial biotransformation product PT-CA in environmental risk assessments.

1. Introduction

Pesticides are ubiquitous environmental pollutants with ecotoxic characteristics, and they have the potential to cause adverse effects on water quality, biodiversity, and human health (Tang et al., 2021). Tolfenpyrad (TFP), a globally used pyrazole insecticide (Chen et al., 2024; JMPR, 2013; Report, 2004), is valued for its high efficiency, broad spectrum, and low infusion factor during tea brewing (Bai et al., 2021; Wei et al., 2017), and it is particularly effective against pests resistant to organophosphates and carbamates (Hikiji et al., 2013; Imada, 2010). However, the proliferation of TFP has led to abundant pesticide residues in the environment (Yu, 2016; Yuan et al., 2017), such as the soil, water, and plants, resulting in ecotoxicity and human exposure risks (Chi et al., 2023; M. Dong et al., 2018; Lan et al., 2022; X. Wang et al., 2022; Wang et al., 2023). For example, TFP residues of 1.0–51.8 mg/kg and 0.4–3.6 mg/kg have been found in green tea and citrus, respectively, with the highest detectable rate and hazard quotient among commonly used pesticides (M. Dong et al., 2018; T. Lin et al., 2022; X. Wu et al., 2023). The dissipation and migration of TFP from field to food result in environmental contamination and potential harm to humans and nontarget organisms, including beneficial insects and economic insects (Q. Wang et al., 2022; Zhang et al., 2022). Aquatic organisms are particularly vulnerable to TFP, with acute and chronic toxicity occurring in various species at extremely low concentrations (Guo et al., 2024; US, 2021). Although cases of fatal TFP poisoning in humans have been reported (Yamaguchi et al., 2012), the toxicity of TFP to humans has not been further investigated.

Biotransformation is a process catalyzed by a set of enzymes, and it plays a crucial role in mediating the toxicity of xenobiotics (Wu et al., 2021). The liver, which contains the most complete metabolic enzymes, is the major site of xenobiotic biotransformation and is a common target organ for xenobiotic-induced toxicity (Ban et al., 2023). Typically, by converting xenobiotics to transformed products with altered physicochemical properties, bioavailability, and biological effects, their toxic effects are reduced, and their excretion from the body is facilitated. However, in some cases, biotransformation can result in the formation of products with similar or more toxic effects, causing greater harm to the body. TFP undergoes extensive biotransformation in plants and animals, rapidly metabolizing in the livers of animals (JMPR, 2013). After a single or 14 daily orally administered to rats, over half of TFP reaches the liver and approximately 90 % of TFP are transformed to PT-CA in plasma, liver and kidney. According to the Joint Meeting on Pesticide Residues evaluation report, TFP is easily biotransformed to tolfenpyrad-benzoic acid (PT-CA), OH-PT-CA, and OH-PT in goats, hens, and rats. Additional reported biotransformation products of TFP in different matrices are shown in the Supporting information (Table S1) (Chen et al., 2024; JMPR, 2013; Wang et al., 2023; Z. Wang et al., 2022; Yamaguchi et al., 2012). In addition, PT-CA and OH-PT, with physiological activities similar to TFP, exhibit stronger acute oral toxicity than their parent TFP in rats (Verger and Boobis, 2013). However, discrepancies may exist in the biotransformation between animal models and humans, and the toxicity elicited by the biotransformation products of TFP remain largely unknown in humans.

Metabolomics coupled with high-resolution mass spectrometry (HRMS) is an efficient tool for the comprehensive analysis of small-molecule endogenous metabolites in biological systems (Guo et al., 2023; S. Lin et al., 2022). Cumulative metabolic changes in response to xenobiotics can serve as indicators of physiological state, with metabolites acting as phenotype modulators, revealing the response pathways that can result in toxicity (Zhang et al., 2020). This approach allows the evaluation of toxicity mechanisms, enabling the identification of potential endogenous biomarkers. Additionally, advancements in HRMS have facilitated the identification and structural characterization of xenobiotic biotransformation products (Lombard-Banek et al., 2021; Xiao et al., 2020). These two approaches utilize many similar instrumental and informatics techniques, both aimed at identifying and characterizing multiple small molecules related to biological systems. Therefore, to gain a comprehensive understanding of the hepatoxicity of TFP, it is essential and feasible to focus on analyzing both xenobiotic biotransformation products and endogenous metabolites while exploring the connections.

In this study, we employed ultra-high-performance liquid chromatography (UHPLC) coupled with HRMS to characterize TFP-induced biotransformation products in human liver microsomes (HLMs) and human liver cells and applied HRMS-based nontargeted metabolomics to analyze endogenous metabolic changes in cells. HLMs, known for their enrichment in cytochrome P450 (CYP) and flavin monooxygenase (FMO), are widely utilized in in vitro xenobiotic metabolism studies (Christia et al., 2022; Luo et al., 2022). HepG2 cells are characterized by their unlimited life span, stable phenotype, and high availability. And HepG2 cells contain biotransformation enzymes homologous to primary human hepatocytes, rendering them an ideal cell line for in vitro metabolism and hepatotoxicity studies (Kiseleva et al., 2023; Y. Wang et al., 2022). Multiple biotransformation products and pathways of TFP were elucidated, some of which were characterized for the first time. In silico toxicity prediction and cell viability assays were performed to primarily assess the hepatic cytotoxicity of TFP and its products. Furthermore, the endogenous metabolic responses induced by TFP and its representative oxidative products, PT-CA, were analyzed and compared in HepG2 cells. By integrating xenobiotic biotransformation and endogenous metabolic analysis, this study provides new insights into the hepatotoxicity of TFP and is expected to guide more in-depth studies on the metabolism and toxic effects of TFP and its biotransformation products in humans.

2. Materials and methods

2.1. HLMs and chemicals

The IPHASE I Metabolic Stability Research Kit (IPHASE Bioscience Co., Ltd., Beijing, China), comprised HLMs (protein concentration 20 mg/mL), a NADPH regeneration system, and phosphate buffer (0.1 M, pH 7.4). The kit, tailored to specific requirements, was stored at –80 °C. The microsomes cytochrome P450 panel included CYP1A2, CYP2A6, CYP2B6, CYP2C8, CYP2C19, CYP2C9, CYP2D6, CYP2E1, CYP3A4/5, and CYP4A11, verified by Sekisui XenoTech. TFP (99.5 % purity) was procured from Alta Scientific (Tianjin, China), while PT-CA (96.6 % purity) was obtained from Dr. Ehenstorfer (Augsburg, Germany). The OH-PT, PT-OH, DS-PT, OH-PT-CHO, DS-PT-OH, OH-PT-OH, and DS-PT-CHO standards were synthesized by Pharmaron Beijing Co., Ltd. (Beijing, China), and the purity of all standards was above 98 %. Formic acid and ammonium formate were purchased from Sigma-Aldrich (St. Louis, MO, USA). Dimethyl sulfoxide (DMSO) and HPLC/MS-grade solvents were obtained from Thermo Fisher Scientific (Waltham, MA, USA).

2.2. HLM incubation experiments

Time-course assessments were performed in parallel in triplicate under the optimized experimental conditions, according to the instructions for the IPHASE I Metabolic Stability Research Kit. Briefly, a

NADPH regeneration system, 0.1 M phosphate buffer, TFP, and liver microsomes were sequentially added into an incubation mixture, followed by 0–3 h incubation at 37 °C in a shaking water bath. An equal volume of ice-cold methanol was added to each sample to terminate the reaction. TFP in DMSO solution was added with final detection concentrations of 0.1, 0.5, 1, 5, 10 μM. Compound Discoverer 3.3 (Thermo Fisher Scientific, Waltham, MA, USA) was used for the identification of biotransformation products. Liquid chromatography was adopted for the determination of biotransformation products using an ACQUITY UPLC HSS T3 column (2.1 × 100 mm, 1.8 μm; Waters Corporation, Milford, MA, USA). The mobile phase consisted of (A) water with 0.1 % formic acid and 1 mM ammonium formate for the aqueous phase and (B) acetonitrile with 0.1 % formic acid for the organic phase. Other chromatographic and mass conditions are listed in Table S2.

2.3. Cell culture and TFP exposure

The HepG2 cells were obtained from Meisen Cell Technology Co., Ltd. (CTCC-001-0014; Zhejiang, China). HepG2 cells were cultured in high-glucose Dulbecco's modified Eagle's medium (DMEM; Gibco, USA), supplemented with 10 % fetal bovine serum (FND500, Excell, Australia) and 1 % penicillin-streptomycin (Macgene, Beijing, China), and maintained in a humidified incubator set at 37 °C with a gas mixture containing 5 % CO_2. HepG2 cells (8×10^6/well) in 8 mL of complete medium were seeded into 10-cm dishes for 24 h of attachment. The cells were exposed in triplicate to TFP at 0.1, 0.5, 1, 5, 10 μM for 0–48 h in complete medium solutions. To avoid DMSO's impact on cell viability, the final concentration of DMSO in the TFP medium solution did not exceed 0.1 %. Post-exposure, the media were transferred into 15 mL centrifuge tubes and stored at –80 °C until processed. The cells were harvested (density: 1×10^7 cells/well) after phosphate-buffered saline (PBS) washing and trypsin digestion and centrifuged at 300 ×*g* for 3 min at 25 °C. The fixed number of cells was resuspended with 100 μL acetonitrile/methanol/water (*v*/v/v, 2:2:1) and then disrupted by three freeze−thaw cycles using liquid nitrogen and centrifuged at 21,130 ×*g* (5 min, 4 °C). Next, the supernatants were collected and subsequently maintained at –80 °C until further analysis. Simultaneously, control groups included dishes with 5 μM TFP complete medium solution without cells and cells exposed to 0.1 % DMSO complete medium solution. No TFP transformation products were observed in control experiments.

2.4. Extraction of TFP biotransformation products from the medium

To extract the extracellular TFP biotransformation products, the culture medium from each dish was transferred to a microcentrifuge tube and centrifuged at 21,130 ×*g* for 5 min at 4 °C. The supernatant (1 mL) was diluted with 4 mL of water and subjected to a cleanup procedure through solid-phase extraction. 3 mL of each sample was passed through Oasis® HLB cartridges (3 cc, 60 mg; Waters, Milford, MA, USA) pre-conditioned sequentially with 3 mL of methanol and 3 mL of water. The cartridges were then washed with 3 mL water to remove salts, dried under a vacuum, and the target compounds were eluted with 3 mL methanol. The 500 μL elution was dried under a nitrogen stream and redissolved in 100 μL of acetonitrile: water (*v*/v, 1:1). The final extraction was centrifuged (21,1300 ×*g*, 5 min, 4 °C) before UHPLC–MS/MS analysis. The exposure medium (1 mL) was spiked with 1 μg/mL tebufenpyrad (N-[(4-*tert*-butylphenyl) methyl]-4-chloro-5-ethyl-2-methylpyrazole-3-carboxamide, CAS 119168-77-3, purity at 99.9 %, 200 ng), a structural analog of TFP, as the surrogate recovery standard prior to dilution.

2.5. Toxicity predictions with ADMETlab 2.0

Structures of TFP and its biotransformation products were generated in the SMILE file format using ChemDraw (PerkinElmer, Waltham, MA) and uploaded to the ADMETlab 2.0 online platform (https://admetmesh.scbdd.com/). The toxicity endpoints of TFP and its products were predicted with hERG blockers, human hepatotoxicity (H-HT), drug induced liver injury (DILI), AMES toxicity, skin sensitization, carcinogencity, and respiratory toxicity. For each endpoint, the output value was the predicted probability of toxicity from inactive (0) to active (1). All data were collected to obtain preliminary insight into the toxicity of the compounds.

2.6. Cell viability assay

HepG2 cell viability was determined using the CellTiter 96 AQueous One Solution Cell Proliferation Assay (Promega, Madison, WI, USA), according to the manufacturer's instructions. MTS (Owen's reagent) underwent biological reduction by living cells to produce a soluble and colored formazan product. To ensure consistent cell viability and condition, all experiments utilized 10 % FBS. Before TFP exposure, cells (2×10^4/well) were seeded and cultured for 24 h in 96-well plates. TFP was first dissolved in DMSO and step-diluted with complete culture media to the exposure concentrations of TFP and PT-CA at 0, 0.1, 0.5, 1, 3, 5, 6, 20, 30, 40, and 50 μM. The dosage gradient corresponded approximately to the environmental concentration observed in water and food. Six replicates were analyzed for each concentration. After TFP or PT-CA exposure for 48 h, the old media were replaced with 100 μL of Owen's reagent and culture media mixture (*v*/v = 1:5) in each well, followed by incubation at 37 °C for 90 min in the absence of light. Absorbance at 490 nm was determined using a microplate reader (SpectraMax i3x, Molecular Devices, Sunnyvale, USA).

2.7. Flow cytometry analysis of apoptosis

Apoptosis was evaluated using the Annexin V-FITC/PI Apoptosis kit (Beyotime Institute of Biotechnology, Shanghai, China). Briefly, HepG2 cells (5×10^5/well) were seeded in 6-well plates, cultured for 24 h, and incubated with 0, 0.5, and 5 μM TFP and PT-CA for 48 h. HepG2 cells, washed with PBS, were trypsin-digested and stained with 5 μL annexin V-FITC and 10 μL PI for 20 min. Subsequently, cells were washed with ice-cold PBS for analysis. Apoptotic cells stained with Annexin V-FITC exhibited green fluorescence, whereas necrotic cells stained with both Annexin V-FITC and PI produced red and green fluorescence. Percentages of cells in the different phases were measured via flow cytometry (BD Accuri TM C6 Plus; Franklin Lakes, NJ, USA). The proportion of apoptotic cells was indicated as a percentage of the sub-Q2 and sub-Q3 fractions in the flow cytometric analysis.

2.8. Nontarget metabolomics analysis

HepG2 cells (density: 8×10^6 cells/well) were seeded into 10-cm dishes, cultured for 24 h, and treated with TFP or PT-CA for 48 h at 0.5 or 5 μM, respectively. The control group medium was replaced with fresh complete culture media. Six replicates were analyzed for each group. For metabolite extraction, all cells were rinsed with PBS, digested with trypsin, and counted using a Countess counter (Invitrogen, Carlsbad, CA, USA) at 1×10^7 cells per sample. The fixed number of cells was quenched with 500 μL ice-cold acetonitrile/methanol/water (*v*/v/v, 2:2:1) containing 100 ng/mL L-Phenyl-d5-alanine as the first internal standard. The samples were then subjected to three freeze−thaw cycles in liquid nitrogen, stood at −20 °C for 2 h, and centrifuged (21,130 ×*g*, 4 °C) for 10 min. The resulting 400 μL supernatants for each group were evaporated to dryness at 10 °C using a vacuum freeze drier (CentriVap, LABCONCO, USA). The residues were resuspended in acetonitrile/water (1:1, *v*/v) containing 500 ng/mL hypoxanthine-d2 as the second internal standard. The samples were then analyzed using an AB SCIEX UHPLC system coupled with a quadrupole time-of-flight mass spectrometer (QTOF MS), using two chromatographic columns in both positive and negative modes. A quality control sample containing a

mixture of all samples was prepared. The instruments and chromatographic separation conditions are listed in Table S3.

2.9. Nontarget metabolomics data processing

In our study, data analysis, including peak picking, alignment, integration, principal component analysis (PCA), and partial least squares discriminant analysis (PLS-DA), was performed using Progenesis QI (version 3.0.3; Waters, Milford, MA, USA) and EZinfo (version 3.0; Waters), as in our previous studies (Jing et al., 2022; Wang et al., 2021). The metabolic profiles of quality control samples with a standard deviation >30 % were excluded to eliminate interference. For each compound, manual assessments were made based on isotope patterns, accurate precursor masses, and fragment spectra of the metabolites compared to authentic standards or theoretical values from the METLIN (http://metlin.scripps.edu/) and HMDB (https://hmdb.ca/) libraries. Molecular weight tolerances of the precursor and fragment were set at 10 ppm. Significantly changed metabolites (ANOVA p-value < 0.05, score in libraries > 35, fold change > 1.5 or fold change < 0.67, and variable importance in the projection value [VIP] >1) were considered differential metabolites resulting from TFP or PT-CA exposure. After peak filtering, spectral library matching, and manual identification, a list of data (mass-to-charge ratio, retention time, and peak intensity) was generated for metabolic pathway analysis using MetaboAnalyst 5.0 (https://www.metaboanalyst.ca/) based on the Kyoto Encyclopedia of Genes and Genomes (KEGG) database.

2.10. Reactive oxygen species (ROS) and mitochondrial membrane potential (MMP) determination

HepG2 cells (1×10^6/well) were cultured in six-well plates for 24 h and then treated with TFP or PT-CA for 48 h, using the same concentrations as those used for the apoptosis analysis. Positive control groups were established, and samples were processed according to the manufacturer's instructions. For ROS detection, 10 μM DCFH-DA (S0033; Beyotime, Shanghai, China) and 2 μM Hoechst 33342 working solution (62,249; Thermo Fisher Scientific, USA) was added to each well for 20 min at 37 °C, followed by washing with serum-free medium. After 48 h of exposure, HepG2 cells were incubated with JC-1 (C2006; Beyotime, Shanghai, China) for MMP detection. The presence of ROS and MMP in the cells was observed using fluorescence microscopy and flow cytometry.

2.11. Targeted metabolomics analysis

For target detection, HepG2 cells (density: 1×10^6 cells/well) were cultured in 6-cm dishes for 24 h and then treated with TFP and PT-CA for 48 h at low and high concentrations. Each sample at 3×10^6 cells for metabolite extraction according to the untargeted metabolomics screening protocol, followed by quenching using 150 μL ice-cold acetonitrile/methanol/water (v/v/v, 2:2:1) and three freeze−thaw cycles in liquid nitrogen and centrifugation (21,130 ×g, 4 °C) for 10 min. The supernatants for each group were equally diluted with acetonitrile containing 0.2 μg/mL internal standard mixture. The optimized declustering potential, collision energy, retention time of the main metabolites in the glutathione and purine metabolic pathways, and internal standards are shown in Table S4 (Alta Scientific, Tianjin, China). The samples were analyzed using an AB SCIEX ultrahigh-performance liquid chromatography system coupled to a QTRAP 6500$^+$ mass spectrometer using multiple reaction monitoring in both positive and negative modes. A quality control sample containing a mixture of all samples was prepared. The detailed instrumentation and chromatographic separation conditions are listed in Table S5.

2.12. Measurement of xanthine oxidase (XO) activity and ATP content

HepG2 cells were seeded into six-well plates at a density of 1×10^6 cells per well, incubated for 24 h, and treated with TFP or PT-CA for 48 h at 0.5 μM and 5 μM. An ATP determination kit (A22066; Thermo Fisher Scientific, USA) and amplex® red xanthine oxidase assay kit (A22182; Thermo Fisher Scientific, USA) were used to measure the concentrations of ATP and XO, respectively, using 1×10^6 cells per sample according to the manufacturers' protocols. The measurements were normalized to the cell concentrations.

3. Results and discussion

3.1. Biotransformation of TFP in HLMs and HepG2 cells

In this study, combination of human liver microsomes (HLMs), which are rich in cytochrome P450 particularly phase I enzymes (J. Dong et al., 2018), with HepG2 cells, abundant in phase II enzymes, were utilized to provide a more comprehensive elucidation for biotransformation of TFP. Initial incubation of HLMs with TFP was performed to simulate the biotransformation process of TFP in the human liver. The characterization of biotransformation products was conducted using a UHPLC-HRMS/MS method, coupled with modified MDF methods and data processing tools, including mass defects, diagnostic ions, fish scores, and isotope patterns (J. Dong et al., 2018). To realize a series of realistic environmental levels, the concentrations of 0.1, 0.5, 1, 5, 10 μM of TFP were tested for more products with our analytical methods. Overall, a total of 14 phase I biotransformed compounds, including hydroxy, oxidative, desaturated, and other products, were characterized, as listed in Table S6. Eight of the products were identified for the first time in this study. The structures of the TFP products were elucidated based on their accurate masses, fragmentation behaviors, and biotransformation patterns (Fig. 1). To enhance confirmation, authentic standards of seven biotransformation products, obtained through chemical synthesis and commercial methods, were employed. The confirmation process involved verifying retention times and mass spectrum data. The possible fragmentation pathways and representative fragments of the products are shown in Fig. 1 and Tables S6–S7.

The parent TFP (m/z 384.14706) eluted at 12.18 min, with the base peak (m/z 197.1005) originating from the amide link break, leading to subsequent breakages producing m/z 107.0490 and m/z 91.0542. Other characteristic fragment ions (m/z 145.0528 and 117.0214) were generated via cleavage of the carbonyl containing a pyrazole ring. Based on the identification of parent compound data, biotransformation products, including the desaturated product M2 (DS-PT m/z 382.1316) and hydroxylated product M7 (OH-PT m/z 400.1420), were easily verified with the same base peak. For M4 (DS-PT-OH m/z 398.1263), distinct fragments from TFP were identified as m/z 211.0757 and m/z 200.0594, attributed to simultaneous desaturation of ethyl on the pyrazole ring and hydroxylation of methyl on diphenylmethane (Table S6). M1 (PT-OH m/z 400.1420) eluted at 9.8 min and generated identical [M + H] + ions as those of OH-PT but with a 16 Da difference from TFP, indicating that it also might be the product of hydroxylation. Distinguishing M1 (PT-OH) from M7 (OH-PT) relied on the base peak ion (m/z 382.1317) and the specific ion (m/z 213.0910) due to the hydroxylation of methyl on diphenylmethane, confirmed by authentic standards. Besides, M1(PT-OH) has an elution time shorter than that of M7(OH-PT). M3 (PT-CA m/z 396.1104) shared similar characteristic fragments with TFP, except for the base peak derived from the carbonyl group. Despite the comparable distribution of characteristic fragments, M14 (OH-PT-CHO m/z 414.1213), the isomer of M3 (PT-CA), was differentiated using authentic standards. Identification of other products with accurate masses and characteristic fragments is presented in Table S6.

We further investigated the biotransformation of TFP in HepG2 cells,

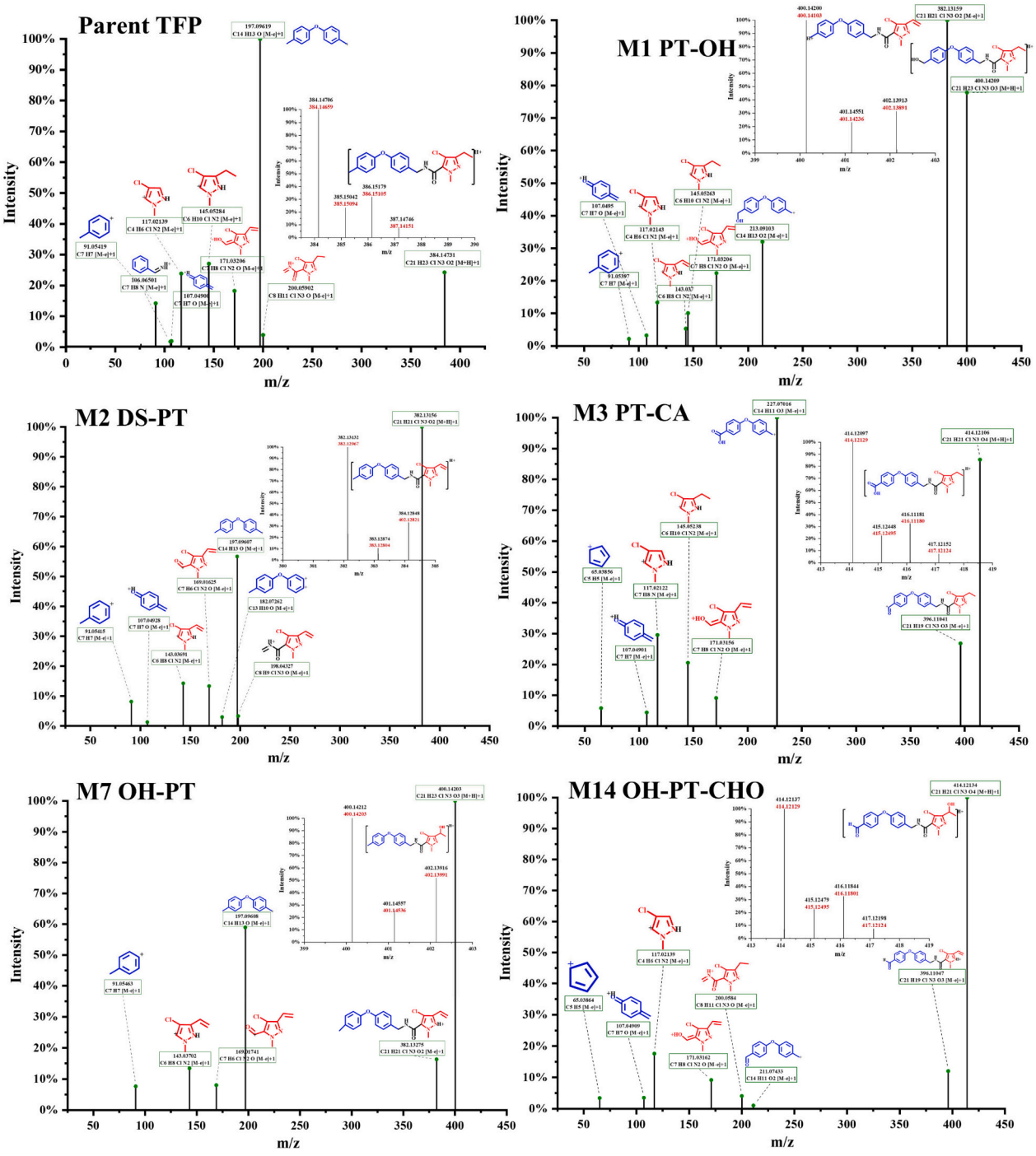

Fig. 1. Representative fragments and fragmentation pathways of TFP biotransformation products revealed by UHPLC-Orbitrap MS in HLMs, and HepG2 cells. MS and MS/MS spectra for other compounds are shown in Tables S6 and S7.

as they cover both phase I and II metabolic pathways and serve as a well-established model of human hepatocyte cells. Based on the same filter conditions for biotransformation in HLMs, a total of 12 biotransformation products were characterized inside HepG2 cells, including eight phase I and four phase II transformation products. Phase II conjugation products were mainly amino acid and taurine conjugation products that have been identified for the first time. The eight phase I transformation products detected in the cells were also present in HLMs, indicating that cytochrome P450 (CYP) enzymes are less abundant in HepG2 cells than in HLMs, aligning with previous reports (Wilkening et al., 2003; Yokoyama et al., 2018). Therefore, the integration of liver microsomes with HepG2 cells facilitates a more comprehensive elucidation for biotransformation of TFP. All biotransformation products found inside the HepG2 cells were also observed in the cell culture medium. The representative fragmentation of the transformation products characterized in the cell and culture media is listed in Table S7.

3.2. Time profiles of TFP biotransformation in HLMs, HepG2 cells, and cell media

In general, the formation and abundance of biotransformation products depend on doses and duration of TFP metabolism. Upon testing with 0.1, 0.5, 1, 5, 10 μM of TFP in HLMs or HepG2 cells, a greater number of products were identified at concentrations above 5 μM, with

TFP still present (Fig. S1A and B). To reveal the temporal profile of TFP metabolism in HLMs, we monitored the main TFP products and their quantities by measuring peak areas at 0, 0.5, 1, 1.5, 2, and 3 h after HLMs incubation with 5 μM TFP. Fig. S1C displays the extracted ion chromatograms of all products at 3 h in HLMs, illustrating the evolution of transformation product during incubation. Retention time validity was confirmed through authentic standards and ChemDraw 20-generated log Kow values. The line graph reveals that the main products included PT-OH, DS-PT, PT-CA, DS-PT-OH, while other products are in trace amounts (Fig. S1D). All products exhibited a consistent increase during the initial period of the incubation, signifying continuous TFP metabolism by HLMs as the incubation progressed. Oxidation predominantly contributed to the transformation process, accounting for approximately half of the total combined peak area, followed by desaturation. Between 1.5 and 3 h, certain products began to decrease, especially PT-OH, T-CHO, and DS-PT. In contrast, PT-CA continued to increase over time, and it surpassed PT-OH and DS-PT by the 3-h mark in HLMs (Fig. S1).

To gain insights into the dynamics and cellular transport of TFP metabolites in HepG2 cells, we conducted a time-dependent analysis of the identified compounds in both cells and culture medium at 5 μM TFP. Fig. 2A illustrates that PT-CA and PT-OH were the predominant intracellular products, akin to HLMs. Following a 6-h TFP exposure, PT-CA peaked within cells, gradually declining and stabilizing from 24 to 48 h. In contrast, PT-OH exhibited a consistent increase throughout the study. In the cell medium, with an overall upward trend, PT-CA levels

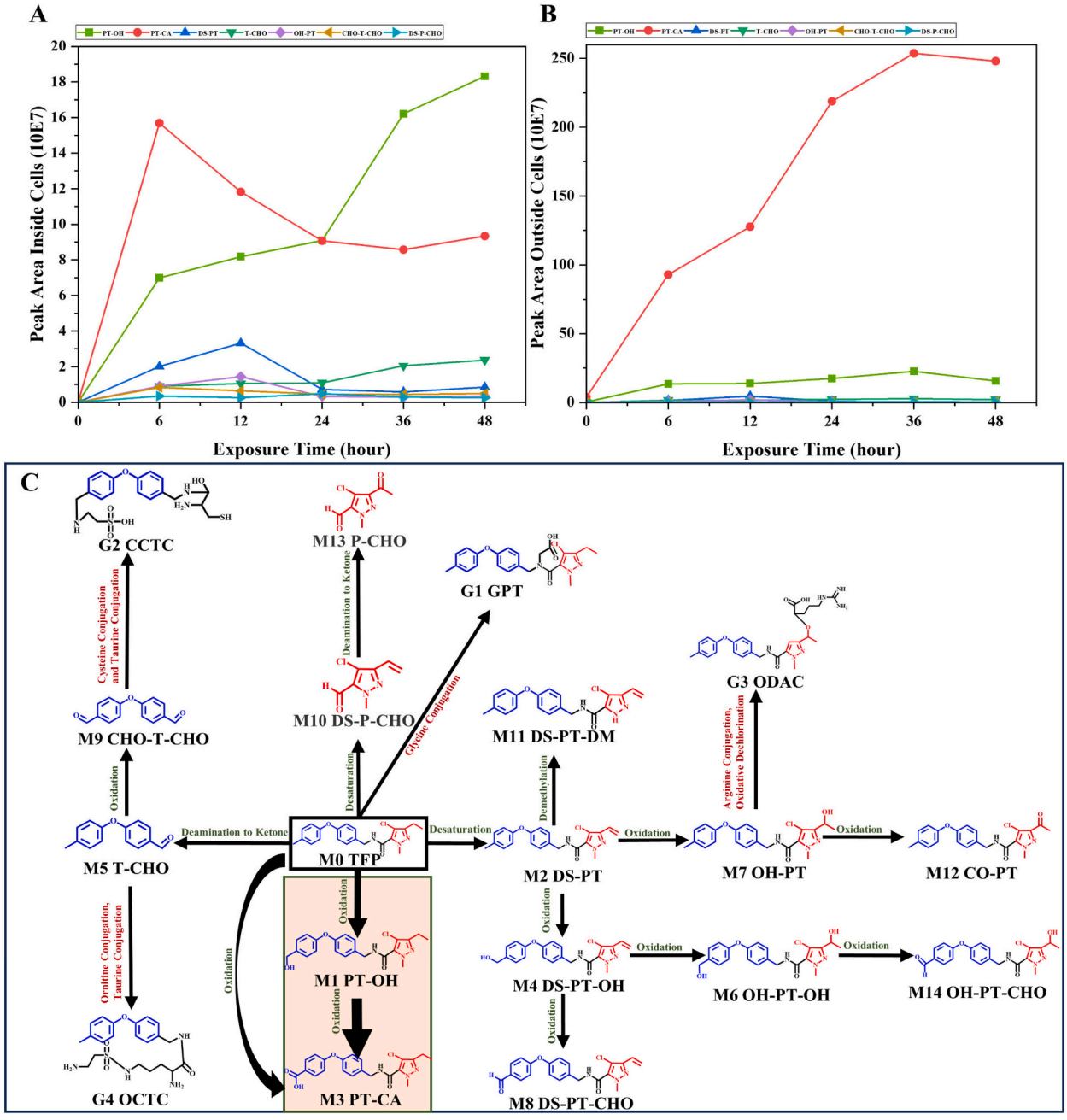

Fig. 2. Biotransformation time profiles and biotransformation pathway of TFP. Trends of phase I biotransformation products content over exposure time inside HepG2 cells (A) and in the culture medium outside cells (B). Proposed TFP biotransformation pathway in vitro human metabolism based on HLMs and HepG2 cells biotransformation (C).
Note: The point values in (A) and (B) represent the means of three replicates calculated by Compound Discover.

increased until 36 h and then decreased slightly, indicating its excretion from the cell. Meanwhile, PT-OH remained at a relatively low level and experienced a rise-and-fall process similar to that of other products (Figs. 2B and S2). These results suggest that the TFP products undergo different cellular transport processes. Nevertheless, PT-CA and PT-OH remained the most abundant biotransformation products in HepG2 cells.

3.3. Proposed hepatic biotransformation pathway of TFP

Based on the characterization of the 14 phase I and four phase II transformation products in HLMs and HepG2 cells, the hepatic biotransformation pathway of TFP was proposed, as shown in Fig. 2C. Briefly, TFP is mainly biotransformed at three positions by hepatic cytochrome P450 enzymes in phase I transformation: oxidation and desaturation of ethyl on the pyrazole ring, oxidation of methyl on diphenylmethyl, and demethylation of the methyl on the pyrazole ring. After the amide bond or C—N bond breaks, the diphenylmethyl (T) and pyrazole rings (P) can be biotransformed independently. In the typical metabolic pattern, PT-OH and PT-CA can both be directly oxidized from TFP and PT-OH can be further oxidized to yield PT-CA (Chen et al., 2024; Hikiji et al., 2013; Imada, 2010). According to our relative quantification results, this process is the dominant pathway. In phase II transformations, the amide bond of TFP can directly bind to glycine, which is the main product of phase II transformation, rather than to other common products catalyzed by sulfotransferases and glucuronosyltransferases in rats (JMPR, 2013). In addition, the aldehyde product T-CHO produced from the oxidation of methyl on diphenylmethyl further conjugates with amino acids and taurine. Similarly, the oxidation product OH-PT can further conjugate with arginine and undergo dechlorination, serving as effective detoxification pathways (Badenhorst et al., 2014; Zabel and Weber, 2015).

In summary, the phase I transformation patterns primarily comprised oxidation, desaturation, demethylation, and C—N or N—O bond breaking, whereas the phase II transformations mainly consisted of amino acid binding and taurine coupling. Overall, these results suggest that the utilization of both HLMs and HepG2 cells provides a more comprehensive investigation of the hepatic biotransformation of TFP. The proposed biotransformation pathway is consistent with human research (Hikiji et al., 2013; Imada, 2010), with our study revealing additional oxidation and demethylation pathways, along with four novel TFP conjugation pathways.

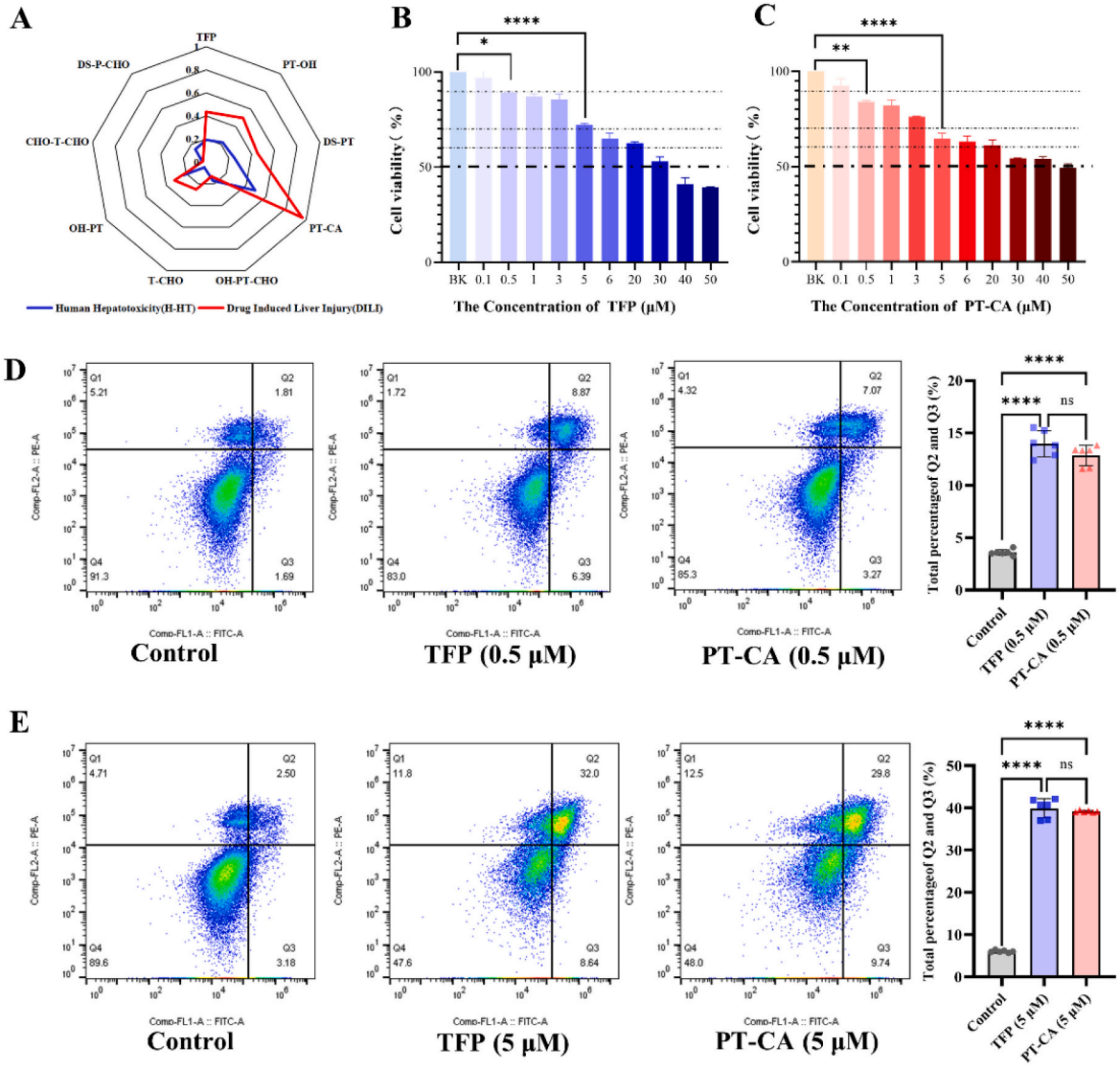

Fig. 3. Hepatoxicity prediction, cell viability, and apoptosis analysis of TFP and PT-CA.(A) Hepatoxicity prediction of TFP and eight products; (B, C) Cell viability assay using an MTS kit in HepG2 cells after 48-h exposure to TFP and PT-CA, respectively. (D, E) Apoptosis analysis of HepG2 cells with flow cytometry after 48-h exposure to TFP and PT-CA, respectively.

3.4. Toxicity prediction and hepatocytotoxicity of TFP and its biotransformation products

The *in silico* ADMETlab 2.0 online platform (https://admetmesh.scbdd.com/) has been widely used to predict the pharmacokinetics and toxicity properties of chemicals, providing ADMET-related endpoints, including physicochemical properties, ADME properties, and toxicity endpoints (Awais et al., 2023; Y. Wu et al., 2023; Xiong et al., 2021). To obtain a preliminary reference for toxicity assessment, TFP and eight biotransformation products found in HLMs, both intracellularly and extracellularly, were uploaded to ADMETlab 2.0. The results of seven toxicity endpoints are shown in detail in Table S8. Fig. 3A visualizes the predicted hepatotoxicity based on the relevant parameters including H-HT and DILI. In the radar chart, the hepatotoxicity of PT-CA (H-HT: 0.489; DILI: 0.962) was significantly greater than that of other transformation products, and also greater than that of the parent drug TFP (H-HT: 0.193; DILI: 0.435). In contrast, the toxicity of PT-OH (H-HT: 0.222; DILI: 0.499) and DS-PT (H-HT: 0.244; DILI: 0.451) was similar to that of TFP. According to our biotransformation study above, PT-CA is one of the most abundant biotransformation products of TFP. Additionally, previous research has identified PT-CA as a major degradation product of TFP in plants and soil, exhibiting cumulative generation upon TFP application (Chen et al., 2024; Report, 2004; Wang et al., 2023). This suggests that the use of TFP can lead to widespread distribution of PT-CA in the environmental system. Collectively, the effects of PT-CA should not be overlooked in hepatotoxicity studies and environmental risk assessments of TFP.

The cell viability and apoptosis of HepG2 cells were evaluated after 48-h exposure to TFP and PT-CA at same gradients, as well as to determine the optimal exposure levels for metabolic analysis and other biological experiments. As shown in Fig. 3B and C, HepG2 cell viability was unaffected by TFP and PT-CA at concentrations below 0.1 μM. A significant drop in viability was evident from 0.5 μM, showing a dose-dependent decline from 0.5 μM to 50 μM. Therefore, after comprehensively considering the environmental doses and biological effects, we selected 0.5 μM (about 0.192 mg/L, lower than the concentration related to the environment) and 5 μM as low-dose and high-dose exposure concentrations for subsequent experiments, resulting in cell viabilities of approximately 90 % and 70 %, respectively. In the flow cytometry analysis, as shown in Fig. 3D and E, the apoptosis of HepG2 cells was significantly increased after exposure to TFP and PT-CA, with apoptosis rates of about 14 % at 0.5 μM of TFP and PT-CA, and a more pronounced apoptotic effect (nearly 40 %) at 5 μM of TFP and PT-CA. Although the apoptotic rates of PT-CA were lower than those of TFP at both concentrations, no significant differences were observed. As evident from the cell viability and apoptosis analyses, both TFP and PT-CA induced lethal effects in HepG2 cells.

3.5. Potential metabolite biomarkers and perturbed metabolic pathways

Following *in silico* predictions and cell viability and apoptosis analyses, the metabolism in HepG2 cells in response to TFP or PT-CA exposure was profiled using nontarget metabolomics to reveal the response pathways that result in toxicity. The PCA model (Fig. S3A–D) demonstrated satisfactory separation between the control and treatment groups in HepG2 cells, suggesting that TFP and PT-CA induced distinct disturbances in the metabolic profiles. After filtering under several conditions (VIP > 1, $p < 0.05$, fold change > 1.5 or fold change < 0.67), approximately 180 metabolites in each treatment group were confirmed as differential metabolites (Figs. S4 and 4A). The volcano plots in Fig. S4 show that there was no significant difference in the amounts of disturbed metabolites between TFP- and PT-CA-treated HepG2 cells despite their doses, and the two compounds perturbed metabolism even at a concentration lower than the environmentally relevant doses. As shown in Fig. 4A, 80 shared metabolites were altered in all groups, and each group had characteristic biomarkers. These shared metabolites, mainly carnitines, organic acids, amino acids, and phospholipids, changed significantly in all treated groups and could be viewed as common biomarkers of TFP or PT-CA exposure (Fig. 4A). In comparison to the control group, the four treated groups exhibited a notable increase in nine metabolites (Fig. 4A). These upregulated metabolites were closely associated with purine and glutathione metabolism, including succinyl-adenosine, oxidized glutathione, and cysteine-glutathione disulfide. Succinyl-adenosine, a product of the dephosphorylation of intracellular adenylosuccinate by 5-nucleotidase, is a biochemical marker of adenylosuccinate lyase deficiency related to purine nucleotide metabolism (Donti et al., 2016; Krijt et al., 1999). The levels of most metabolites consistently declined in all four treatment groups. Several metabolites were involved in the TCA cycle, including citric acid, D-fructose 1-phosphate, fructose 6-phosphate and oxoglutaric acid. The inhibition of the TCA cycle after exposure to TFP or PT-CA suggests the perturbation of energy metabolism.

The significantly altered metabolites (Tables S9–S12) in each group were further aggregated using MetaboAnalyst 5.0 (https://www.metaboanalyst.ca/) for pathway analysis. Based on the KEGG pathway database of *Homo sapiens*, we found that the significantly perturbed metabolites after TFP or PT-CA intervention were highly associated with perturbations in the glycerophospholipid metabolism, purine metabolism, alanine, aspartate, glutamate metabolism, phenylalanine metabolism, pyrimidine metabolism, butanoate metabolism, glutathione metabolism and TCA cycle at both low and high doses (Fig. 4B–E). The top 10 pathways (pathway impact > 0.1 and $p < 0.05$) in each group shared similar distributions, differing mainly in the levels of impact. Purine metabolism is an essential pathway related to oxidative stress, and an imbalance between purine salvage and biosynthesis can lead to the production of ROS (Tian et al., 2022). Additionally, in the mitochondria, glutathione metabolism is a key pathway against oxidative stress, protecting cells from oxidative damage (Cassier-Chauvat et al., 2023; Gao et al., 2023) and further inhibiting the excessive production of ROS. Therefore, the perturbed pathways discussed herein provide new insights into the metabolic interference of TFP and PT-CA in HepG2 cells, particularly those related to oxidative stress in mitochondria.

3.6. Mitochondrial damage induced by TFP and PT-CA

We further investigated the potential toxicity and underlying mechanisms of TFP and PT-CA on mitochondrial dysfunction. Mitochondrial damage is often characterized by a decrease in the overproduction of ROS and a decrease in MMP, resulting in apoptosis (Yitzhaki et al., 2007). Thus, we explored ROS production after exposure to TFP and PT-CA. As shown in Figs. 5A and S5, ROS generation increased in a dose-dependent manner following TFP and PT-CA treatment, with changes visible even after exposure to low doses of TFP and PT-CA. Extra ROS after TFP and PT-CA exposure contributed to the generation of a pro-oxidative environment. Furthermore, an MMP assay employing JC-1 cyanine dye was conducted using flow cytometry (Fig. 5B and C) and fluorescence microscopy (Fig. S5). The transition from red (JC-1 aggregates) to green (JC-1 monomers) fluorescence indicated a decline in MMP. After exposure to low doses of TFP or PT-CA, approximately 85 % of HepG2 contained JC-1 aggregates, which was lower than that of the control group (approximately 95 %). After being treated with high doses, the percentage of JC-1 aggregates substantially declined to about 65 %. Taken together, the changes in ROS and MMP indicate oxidative stress in the mitochondria, an imbalance of intracellular redox status, and further exacerbated mitochondrial dysfunction within HepG2 cells (A. Y.-T. Wu et al., 2023).

Mitochondria also play a central role in the cellular metabolic network, where purine and glutathione metabolism occur and ATP is generated (Griffiths et al., 2010). We focused on NAD, NADH, and 11 purine metabolites, identified and quantified using standards (Figs. 5D and S6A). Among them, 10 metabolites showed a dose-dependent increase in TFP- or PT-CA-treated HepG2 cells, demonstrating a consistent

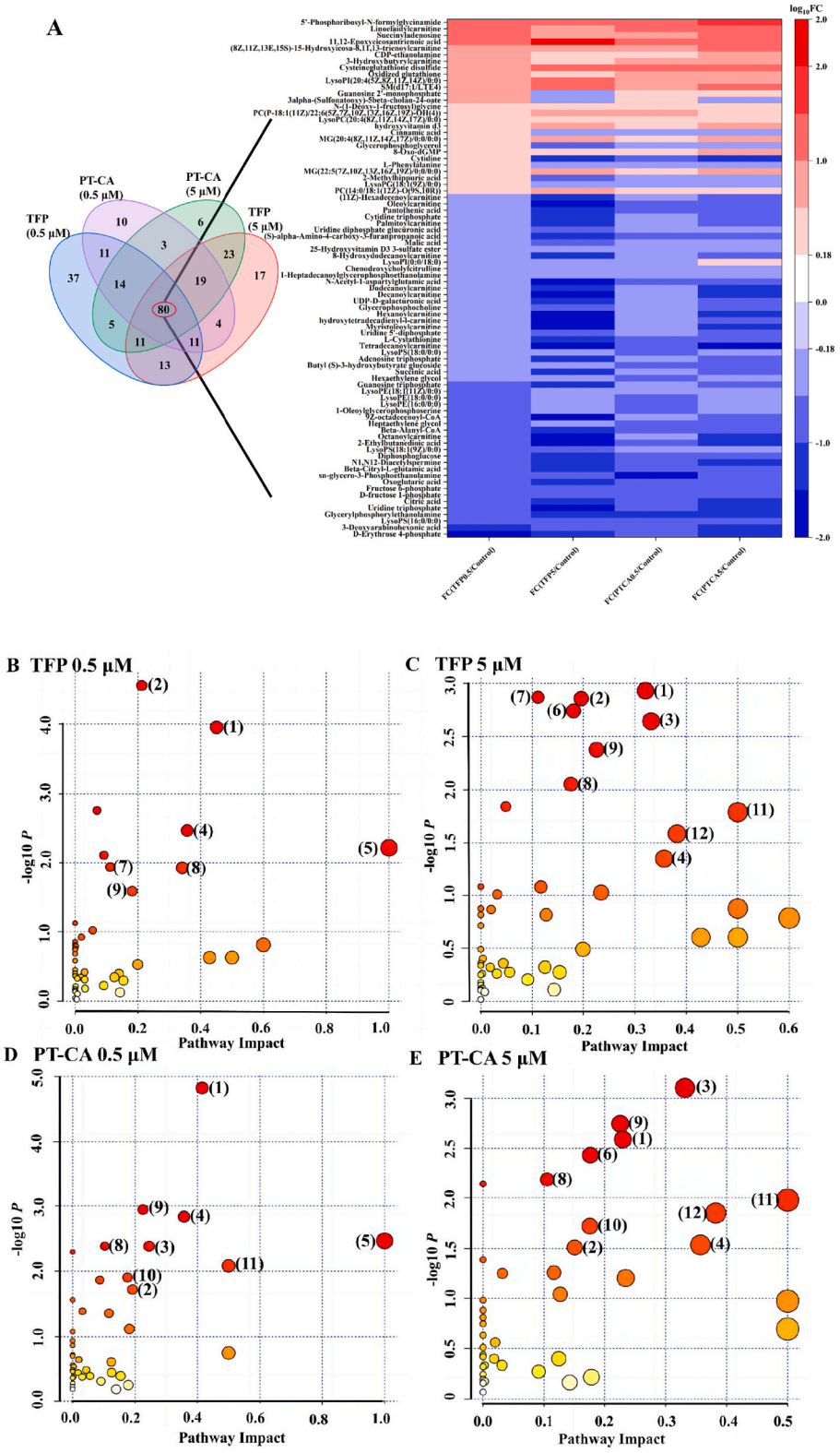

Fig. 4. Potential metabolite biomarkers and different perturbed metabolic pathways induced by TFP or PT-CA. (A)Venn and heatmap showing potential metabolite biomarkers after TFP or PT-CA exposure, ranked by descending fold change of TFP at low concentration. (B) Perturbed metabolic pathways reveal possible mechanisms of toxicity.

Note: (1) Glycerophospholipid metabolism; (2) Purine metabolism; (3) Alanine, aspartate, and glutamate metabolism; (4) Phenylalanine metabolism; (5) Phenylalanine, tyrosine and tryptophan biosynthesis; (6) Pyrimidine metabolism; (7) Butanoate metabolism; (8) Glutathione metabolism; (9) Citrate cycle (TCA cycle); (10) Arginine and proline metabolism; (11) D-Glutamine and D-glutamate metabolism; (12) Pantothenate and CoA biosynthesis.

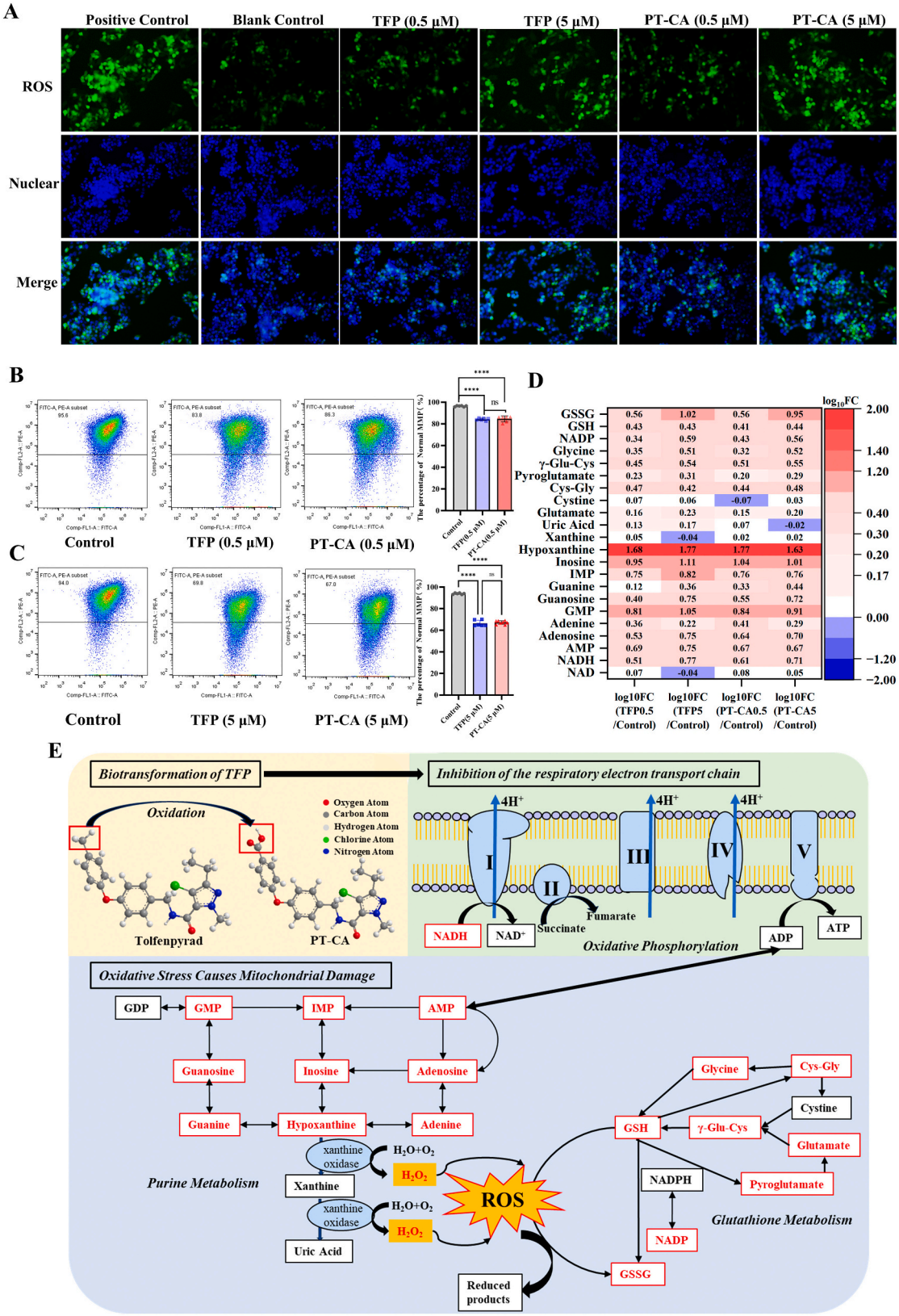

Fig. 5. Mitochondrial damage induced by TFP and PT-CA. (A) Visualization of ROS via fluorescence microscopy. (B, C) MMP assay using flow cytometry. The upper portion indicates normal MMP, and the lower portion of the cell cluster indicates a decrease in membrane potential. In comparison to the control group via one-way ANOVA, $n = 6$, ****:$P < 0.001$ compared with the blank control group. (D) TFP and PT-CA disturb purine and glutathione metabolism in HepG2 cells. Metabolites that significantly increased are annotated in red, while other metabolites with no significance or no detection are in black. See Supplementary material Fig. S6 for specific fold change values. (E) TFP and its important product PT-CA lead to oxidative stress related to mitochondria damage.

trend. The increase in NADH and reduction in NAD suggested the inhibition of the electron transport chain, hindering the conversion of NADH to NAD (Kulthawatsiri et al., 2023; Mishra et al., 2023). The inhibitory effect on mitochondrial respiration triggers a chain of subsequent reactions, resulting in the disruption of ATP synthesis in the mitochondria. A considerable decrease in ATP production was observed after exposure to TFP or PT-CA (Fig. S6B). Moreover, the accumulation of AMP, the ultimate downstream product of ATP, suggested diminished energy levels, resulting in a series of electron transport chain abnormalities. Furthermore, the substantial increase in nucleotides and their precursor substances led to a significant alteration in hypoxanthine content (Fig. 5D). The heightened hypoxanthine content, derived from AMP degradation under hypoxic conditions and oxygen limitation, serves as an oxidative stress biomarker (Kirk Cochran et al., 2019; Lembo et al., 2021). Notably, XO oxidized hypoxanthine and xanthine, producing hydrogen peroxide (H_2O_2) and superoxide (Veljković et al., 2020). XO activity was increased significantly after TFP or PT-CA exposure in HepG2 cells (Fig. S6C); therefore, high levels of hypoxanthine and XO enhanced ROS production.

Additionally, we analyzed nine metabolites related to glutathione metabolism, a key antioxidant pathway in mitochondria, using their standards (Fig. 5D). As shown in Fig. 5D, the levels of most metabolites in this pathway showed an obvious upward trend in the TFP- and PT-CA-treated groups. This pathway begins with cystine and glutamate and ends with oxidized glutathione in HepG2 cells; the conversion between reduced and oxidized glutathione (GSH and GSSG) is a critical step in antioxidation (Lou, 2022). To produce as much GSH as possible, other metabolites are significantly increased, and GSH is ultimately converted to abundant GSSG to defend against oxidative damage. Upregulation of the glutathione pathway is a factor involved in suppression of ROS levels and protection against oxidative stress-induced injuries in TFP- or PT-CA-treated HepG2 cells. In conclusion, targeted metabolomics revealed variations consistent with those of nontargeted metabolomics in purine and glutathione metabolism, providing a more comprehensive and accurate quantification of the metabolites related to oxidative stress and mitochondrial damage.

The enzymatic activity in HepaRG cells was comparable to that in human primary hepatocytes, indicating that HepaRG cells are good models for studying drug metabolism and toxicity (Yokoyama et al., 2018). In this study, HepaRG cells were utilized for validating certain critical toxicity endpoints. The cell viability of HepaRG cells was evaluated after a 48-h exposure to TFP and PT-CA at same gradients. As shown in Fig. S7A–B, HepaRG cell viability significantly reduced, starting at 0.5 μM, exhibiting a dose-dependent decline from 0.5 μM to 50 μM, a pattern similar to that observed in HepG2 cells. Furthermore, we focused on purine metabolism and glutathione metabolism associated with mitochondrial damage in HepaRG cells. Our results revealed that nine metabolites of the two pathways showed increase in TFP- or PT-CA-treated HepaRG cells (Fig. S7C). Particularly, the heightened level of hypoxanthine content in HepaRG cells, resulting from nucleotide degradation, also can serve as a biomarker of oxidative stress similar to what was observed in HepG2 cells (Kirk Cochran et al., 2019; Lembo et al., 2021). Moreover, the elevated levels of NADP and GSSG provide evidence of oxidative stress and mitochondrial damage (Lou, 2022). The results showed that TFP and PT-CA induced lethal effects and disrupt purine metabolism and glutathione metabolism in HepaRG cells, with comparative toxicity observed in HepG2 cells. Therefore, the critical endpoints mentioned above suggest that TFP and PT-CA exhibit hepatotoxicity in HepG2 and HepaRG cells.

Possible mechanisms of TFP-induced hepatotoxicity are shown in Fig. 5E. As a xenobiotic, TFP is biotransformed by cytochrome P450 enzymes, resulting in a series of biotransformation products. Among these products, PT-CA remained stable, abundant, and exhibited toxicity similar to that of the parent TFP. TFP and PT-CA exert similar effects by inhibiting the electron transport chain, which leads to disorders in energy metabolism and ROS overproduction, causing mitochondrial dysfunction. As an adaptive response, purine and glutathione metabolism were upregulated. These metabolic disorders can enhance ROS overproduction and exacerbate oxidative damage. The present study demonstrates the advantage of integrating xenobiotic biotransformation and endogenous metabolic analysis in toxicological research. It also provides new insights into the hepatotoxicity of TFP and offers valuable guidance for in-depth studies into the metabolism and toxic effects of TFP and its important oxidative product, PT-CA, in humans.

4. Conclusions

This study provides the first comprehensive report on the biotransformation of TFP in humans and elucidates its possible transformation pathways. These results suggest that TFP is easily and abundantly biotransformed into its oxidative product PT-CA, which is stable and not easily eliminated over long periods. Preliminary toxicity prediction and hepatocytotoxicity assessment revealed them similar toxic and lethal effects in HepG2 cells. Further metabolic studies revealed common potential metabolite biomarkers and perturbations in multiple metabolic pathways following TFP or PT-CA exposure. All results indicated that environmentally relevant doses of TFP and PT-CA act in similar ways in human hepatocytes, both inducing oxidative stress related to mitochondrial damage and cell death and causing the upgradation of purine and glutathione metabolism. Therefore, this study provides novel insights that could enhance our understanding of the metabolic mechanisms underlying the response to TFP, particularly in mitochondria-related response pathways, emphasizing the non-negligible toxicity of its biotransformation product PT-CA in environmental risk assessments.

Funding

This research did not receive any specific grants from funding agencies in the public, commercial, or not-for-profit sectors.

CRediT authorship contribution statement

Xin Jiang: Writing – original draft, Validation, Methodology, Investigation, Conceptualization. **Yingjie Zhu:** Writing – review & editing, Validation, Methodology, Investigation, Conceptualization. **Suhe Dong:** Validation, Funding acquisition. **Runfeng Lin:** Methodology. **Peihong Zhu:** Validation. **Jie Mao:** Data curation. **Yanqing Cao:** Data curation. **Xiaoyao Yin:** Software. **Fangting Dong:** Validation. **Kun He:** Writing – review & editing, Project administration. **Na Wang:** Writing – review & editing, Project administration.

Declaration of competing interest

The authors declare that they have no known competing financial interests or personal relationships that could have appeared to influence the work reported in this paper.

Data availability

Data will be made available on request.

Appendix A. Supplementary data

Supplementary data to this article can be found online at https://doi.org/10.1016/j.scitotenv.2024.175320.

References

Awais, M., Akter, R., Boopathi, V., Ahn, J.C., Lee, J.H., Mathiyalagan, R., Kwak, G.-Y., Rauf, M., Yang, D.C., Lee, G.S., Kim, Y.-J., Jung, S.-K., 2023. Discrimination of Dendropanax morbifera via HPLC fingerprinting and SNP analysis and its impact on obesity by modulating adipogenesis- and thermogenesis-related genes. Front. Nutr. 10 https://doi.org/10.3389/fnut.2023.1168095.

Badenhorst, C.P.S., Erasmus, E., van der Sluis, R., Nortje, C., van Dijk, A.A., 2014. A new perspective on the importance of glycine conjugation in the metabolism of aromatic acids. Drug Metab. Rev. 46, 343–361. https://doi.org/10.3109/03602532.2014.908903.

Bai, A., Chen, A., Chen, W., Liu, S., Luo, X., Liu, Y., Zhang, D., 2021. Residue behavior, transfer and risk assessment of tolfenpyrad, dinotefuran and its metabolites during tea growing and tea brewing. J. Sci. Food Agric. 101, 5992–6000. https://doi.org/10.1002/jsfa.11253.

Ban, K., Imai, K., Oyama, S., Tokunaga, J., Ikeda, Y., Uchiyama, H., Kadota, K., Tozuka, Y., Akai, S., Sawama, Y., 2023. Sulfonium salt reagents for the introduction of deuterated alkyl groups in drug discovery. Angew. Chem. Int. Ed. 62 https://doi.org/10.1002/anie.202311058.

Cassier-Chauvat, C., Marceau, F., Farci, S., Ouchane, S., Chauvat, F., 2023. The glutathione system: a journey from Cyanobacteria to higher eukaryotes. Antioxidants 12, 1199. https://doi.org/10.3390/antiox12061199.

Chen, S., Ye, Y., Liao, F., Wu, S., Zhang, K., 2024. Insight into the uptake, translocation, metabolism, dissipation and risk assessment of tolfenpyrad in romaine and edible amaranth grown in hydroponic conditions. Food Chem. 437, 137896 https://doi.org/10.1016/j.foodchem.2023.137896.

Chi, D., Wang, W., Mu, S., Chen, S., Zhang, K., 2023. Computer-aided prediction, synthesis, and characterization of magnetic molecularly imprinted polymers for the extraction and determination of Tolfenpyrad in lettuce. Foods 12, 1045. https://doi.org/10.3390/foods12051045.

Christia, C., da Silva, K.M., Poma, G., van Nuijs, A.L.N., Covaci, A., 2022. In vitro phase I metabolism of newly identified plasticizers using human liver microsomes combined with high resolution mass spectrometry and based on non-targeted and suspect screening workflows. Toxicol. Lett. 356, 33–40. https://doi.org/10.1016/j.toxlet.2021.12.005.

Dong, J., Fernández-Fueyo, E., Hollmann, F., Paul, C.E., Pesic, M., Schmidt, S., Wang, Y., Younes, S., Zhang, W., 2018. Biocatalytic oxidation reactions: a Chemist's perspective. Angew. Chem. Int. Ed. 57, 9238–9261. https://doi.org/10.1002/anie.201800343.

Dong, M., Wen, G., Tang, H., Wang, T., Zhao, Z., Song, W., Wang, W., Zhao, L., 2018. Dissipation and safety evaluation of novaluron, pyriproxyfen, thiacloprid and tolfenpyrad residues in the citrus-field ecosystem. Food Chem. 269, 136–141. https://doi.org/10.1016/j.foodchem.2018.07.005.

Donti, T.R., Cappuccio, G., Hubert, L., Neira, J., Atwal, P.S., Miller, M.J., Cardon, A.L., Sutton, V.R., Porter, B.E., Baumer, F.M., Wangler, M.F., Sun, Q., Emrick, L.T., Elsea, S.H., 2016. Diagnosis of adenylosuccinate lyase deficiency by metabolomic profiling in plasma reveals a phenotypic spectrum. Mol. Genet. Metab. Rep. 8, 61–66. https://doi.org/10.1016/j.ymgmr.2016.07.007.

Gao, R., Jiang, Z., Wu, X., Cai, Z., Sang, N., 2023. Metabolic regulation of tumor cells exposed to different oxygenated polycyclic aromatic hydrocarbons. Sci. Total Environ. 167833 https://doi.org/10.1016/j.scitotenv.2023.167833.

Griffiths, W.J., Koal, T., Wang, Y., Kohl, M., Enot, D.P., Deigner, H.-P., 2010. Targeted metabolomics for biomarker discovery. Angew. Chem. Int. Ed. 49, 5426–5445. https://doi.org/10.1002/anie.200905579.

Guo, Y., Ji, S., Li, D., Sang, N., 2023. Ambient NO2 exposure affects hepatic glycolipid metabolism in mice with a sex-dependent property. J. Hazard. Mater. 441, 129957 https://doi.org/10.1016/j.jhazmat.2022.129957.

Guo, Y., Zhang, T., Wang, X., Zhang, J., Miao, W., Li, Q.X., Fan, Y., 2024. Toxic effects of the insecticide tolfenpyrad on zebrafish embryos: cardiac toxicity and mitochondrial damage. Environ. Toxicol. https://doi.org/10.1002/tox.24133.

Hikiji, W., Yamaguchi, K., Saka, K., Hayashida, M., Ohno, Y., Fukunaga, T., 2013. Acute fatal poisoning with Tolfenpyrad. Journal of forensic and legal medicine. England. https://doi.org/10.1016/j.jflm.2013.08.012.

Imada, Y., 2010. Acute tebufenpyrad and tolfenpyrad poisoning in humans. Chudoku Kenkyu 23 (4), 324–328. Japanese.

Jing, N., Peng, J., Yang, X., Wang, X., Liu, Q., Wang, H., Li, W., Dong, F., He, K., Wang, N., 2022. Metabolomics analysis of chronic exposure to Dimethylarsenic acid in mice and toxicity assessment of organic arsenic in food. ACS Omega 7, 35774–35782. https://doi.org/10.1021/acsomega.2c03806.

JMPR, 2013. P. residues. In: Tolfenpyrad (Available online: https://apps.who.int/pesticide-residues-jmpr-database/pesticide?name=TOLFENPYRAD (accessed: June 10, 2024)).

Kirk Cochran, J., Bokuniewicz, H.J., Yager, P.L., 2019. Preface to Encyclopedia of Ocean Sciences, Third Edition, in: Encyclopedia of Ocean Sciences. Elsevier, p. vii. https://doi.org/10.1016/b978-0-12-813081-0.09961-4.

Kiseleva, O.I., Kurbatov, I.Y., Arzumanian, V.A., Ilgisonis, E.V., Zakharov, S.V., Poverennaya, E.V., 2023. The expectation and reality of the HepG2 Core metabolic profile. Metabolites 13, 908. https://doi.org/10.3390/metabo13080908.

Krijt, J., Kmoch, S., Hartmannová, H., Havlíček, V., Šebesta, I., 1999. Identification and determination of succinyladenosine in human cerebrospinal fluid. J. Chromatogr. B Biomed. Sci. Appl. 726, 53–58. https://doi.org/10.1016/s0378-4347(99)00024-9.

Kulthawatsiri, T., Kittirat, Y., Phetcharaburanin, J., Tomacha, J., Promraksa, B., Wangwiwatsin, A., Klanrit, P., Titapun, A., Loilome, W., Namwat, N., 2023. Metabolomic analyses uncover an inhibitory effect of niclosamide on mitochondrial membrane potential in cholangiocarcinoma cells. PeerJ 11, e16512. https://doi.org/10.7717/peerj.16512.

Lan, T., Yang, G., Li, J., Chi, D., Zhang, K., 2022. Residue, dissipation and dietary intake risk assessment of tolfenpyrad in four leafy green vegetables under greenhouse conditions. Food Chem. X 13, 100241. https://doi.org/10.1016/j.fochx.2022.100241.

Lembo, C., Buonocore, G., Perrone, S., 2021. Oxidative Stress in Preterm Newborns. Antioxidants 10, 1672. https://doi.org/10.3390/antiox10111672.

Lin, S., Zhang, H., Wang, C., Su, X.-L., Song, Y., Wu, P., Yang, Z., Wong, M.-H., Cai, Z., Zheng, C., 2022. Metabolomics reveal Nanoplastic-induced mitochondrial damage in human liver and lung cells. Environ. Sci. Technol. https://doi.org/10.1021/acs.est.2c03980.

Lin, T., Chen, X.-L., Guo, J., Li, Meng-Xia, Tang, Y.-F., Li, Mao-Xuan, Li, Y.-G., Cheng, L., Liu, H.-C., 2022. Simultaneous determination and health risk assessment of four high detection rate pesticide residues in Pu'er tea from Yunnan. China. Molecules 27, 1053. https://doi.org/10.3390/molecules27031053.

Lombard-Banek, C., Li, J., Portero, E.P., Onjiko, R.M., Singer, C.D., Plotnick, D., Al Shabeeb, R.Q., Nemes, P., 2021. *In Vivo* Subcellular Mass Spectrometry Enables Proteo-Metabolomic Single-cell Systems Biology in a Chordate Embryo Developing to a Normally Behaving Tadpole (*X. laevis*). bioRxiv. https://doi.org/10.1101/2021.01.19.426900.

Lou, M.F., 2022. Glutathione and Glutaredoxin in redox regulation and cell signaling of the Lens. Antioxidants 11, 1973. https://doi.org/10.3390/antiox11101973.

Luo, X., Lin, L., Abdallah, M.A.-E., Chen, L.-J., Mai, B., Harrad, S., 2022. Comparative in vitro metabolism of short chain chlorinated Paraffins (Sccps) by human and chicken liver Microsomes: first insight into Heptachlorodecanes. SSRN Journal. https://doi.org/10.2139/ssrn.4089839.

Mishra, S., Welch, N., Karthikeyan, M., Bellar, A., Musich, R., Singh, S.S., Zhang, D., Sekar, J., Attaway, A.H., Chelluboyina, A.K., Lorkowski, S.W., Roychowdhury, S., Li, L., Willard, B., Smith, J.D., Hoppel, C.L., Vachharajani, V., Kumar, A., Dasarathy, S., 2023. Dysregulated cellular redox status during hyperammonemia causes mitochondrial dysfunction and senescence by inhibiting sirtuin-mediated deacetylation. Aging Cell 22. https://doi.org/10.1111/acel.13852.

Report, E., 2004. Food safety commission pesticides expert committee evaluation report: Tolfenpyrad. Food safety commission pesticides expert committee 01, 1–40. Available online. https://www.fsc.go.jp/english/evaluationreports/. (Accessed 10 June 2024).

Tang, F.H.M., Lenzen, M., McBratney, A., Maggi, F., 2021. Risk of pesticide pollution at the global scale. Nat. Geosci. 14, 206–210. https://doi.org/10.1038/s41561-021-00712-5.

Tian, R., Yang, C., Chai, S., Guo, H., Seim, I., Yang, G., 2022. Evolutionary impacts of purine metabolism genes on mammalian oxidative stress adaptation. https://doi.org/10.24272/j.issn.2095-8137.2021.420.

US, E, 2021. Aquatic Life Benchmarks Ecological Risk Assessments for Registered Pesticides. Available. online. https://www.epa.gov/pesticide-science-and-assessing-pesticide-risks/aquatic-life-benchmarks-and-ecological-risk.

Veljković, A., Hadži-Dokić, J., Sokolović, D., Bašić, D., Veličković-Janković, L., Stojanović, M., Popović, D., Kocić, G., 2020. Xanthine oxidase/dehydrogenase activity as a source of oxidative stress in prostate Cancer tissue. Diagnostics. (Basel). 10, 668. https://doi.org/10.3390/diagnostics10090668.

Verger, P.J.P., Boobis, A.R., 2013. Reevaluate pesticides for food security and safety. Science 341, 717–718. https://doi.org/10.1126/science.1241572.

Wang, Q., Sun, Z., Huang, Z., Ma, S., Chen, K., Ju, X., 2022. Effects of tolfenpyrad exposure on development and response mechanism in the silkworm. *Bombyx mori*. Pestic Biochem Physiol 189, 105280. https://doi.org/10.1016/j.pestbp.2022.105280.

Wang, S., Yang, X., Liu, F., Wang, X., Zhang, X., He, K., Wang, H., 2021. Comprehensive Metabolomic analysis reveals dynamic metabolic reprogramming in Hep3B cells with aflatoxin B1 exposure. Toxins. (Basel). 13, 384. https://doi.org/10.3390/toxins13060384.

Wang, X., Zhang, X., Wang, Z., Zhou, L., Luo, F., Chen, Z., 2022. Dissipation behavior and risk assessment of tolfenpyrad from tea bushes to consuming. Sci. Total Environ. 806, 150771 https://doi.org/10.1016/j.scitotenv.2021.150771.

Wang, Y., Ning, X., Li, G., Sang, N., 2022. New insights into potential estrogen agonistic activity of triazole fungicides and coupled metabolic disturbance. J. Hazard. Mater. 424, 127479 https://doi.org/10.1016/j.jhazmat.2021.127479.

Wang, Z., Wang, M., Li, Z., Zhou, L., Zhang, X., Yang, M., Sun, H., Chen, Z., Luo, F., Wang, X., 2022. Establishment of a QuEChERS-UPLC-MS/MS method for simultaneously detecting Tolfenpyrad and its metabolites in tea. SSRN Journal. https://doi.org/10.2139/ssrn.4164567.

Wang, Z., Luo, F., Guo, M., Yu, J., Zhou, L., Zhang, X., Sun, H., Yang, M., Lou, Z., Chen, Z., Wang, X., 2023. The metabolism and dissipation behavior of tolfenpyrad in tea: a comprehensive risk assessment from field to cup. Sci. Total Environ. 877, 162876 https://doi.org/10.1016/j.scitotenv.2023.162876.

Wei, Q., Mu, X.-C., Yu, H.-Y., Niu, C.-D., Wang, L.-X., Zheng, C., Chen, Z., Gao, C.-F., 2017. Susceptibility of Empoasca vitis (Hemiptera: Cicadellidae) populations from the main tea-growing regions of China to thirteen insecticides. Crop Prot. 96, 204–210. https://doi.org/10.1016/j.cropro.2017.02.021.

Wilkening, S., Stahl, F., Bader, A., 2003. Comparison of primary human hepatocytes and hepatoma cell line HepG2 with regard to their biotransformation properties. Drug Metab. Dispos. 31, 1035–1042. https://doi.org/10.1124/dmd.31.8.1035.

Wu, A.Y.-T., Sekar, P., Huang, D.-Y., Hsu, S.-H., Chan, C.-M., Lin, W.-W., 2023. Spatiotemporal roles of AMPK in PARP-1- and autophagy-dependent retinal pigment epithelial cell death caused by UVA. J. Biomed. Sci. 30 https://doi.org/10.1186/s12929-023-00978-4.

Wu, M., Li, G., Li, P., Jiang, N., Wei, S., Petropoulos, E., Li, Z., 2021. Assessing the ecological risk of pesticides should not ignore the impact of their transformation byproducts – the case of chlorantraniliprole. J. Hazard. Mater. 418, 126270 https://doi.org/10.1016/j.jhazmat.2021.126270.

Wu, X., Xie, Y., Tong, K., Chang, Q., Hu, X., Fan, C., Chen, H., 2023. Simultaneous screening and quantification of 479 pesticides in green tea by LC-QTOF-MS. Foods 12, 4177. https://doi.org/10.3390/foods12224177.

Wu, Y., Ma, Y., Cao, J., Xie, R., Chen, F., Hu, W., Huang, Y., 2023. Feasibility study on the use of "Qi-tonifying medicine compound" as an anti-fatigue functional food

ingredient based on network pharmacology and molecular docking. Front. Nutr. 10 https://doi.org/10.3389/fnut.2023.1131972.
Xiao, L., Wang, C., Dai, C., Littlepage, L.E., Li, J., Schultz, Z.D., 2020. Untargeted tumor metabolomics with liquid chromatography–surface-enhanced Raman spectroscopy. Angew. Chem. Int. Ed. 59, 3439–3443. https://doi.org/10.1002/anie.201912387.
Xiong, G., Wu, Z., Yi, J., Fu, L., Yang, Z., Hsieh, C., Yin, M., Zeng, X., Wu, C., Lu, A., Chen, X., Hou, T., Cao, D., 2021. ADMETlab 2.0: an integrated online platform for accurate and comprehensive predictions of ADMET properties. Nucleic Acids Res. 49, W5–W14. https://doi.org/10.1093/nar/gkab255.
Yamaguchi, K., Hikiji, W., Takino, M., Saka, K., Hayashida, M., Fukunaga, T., Ohno, Y., 2012. Analysis of Tolfenpyrad and its metabolites in plasma in a Tolfenpyrad poisoning case. J. Anal. Toxicol. 36, 529–537. https://doi.org/10.1093/jat/bks060.
Yitzhaki, S., Hochhauser, E., Porat, E., Shainberg, A., 2007. Uridine-5′-triphosphate (UTP) maintains cardiac mitochondrial function following chemical and hypoxic stress. J. Mol. Cell. Cardiol. 43, 653–662. https://doi.org/10.1016/j.yjmcc.2007.07.060.
Yokoyama, Y., Sasaki, Y., Terasaki, N., Kawataki, T., Takekawa, K., Iwase, Y., Shimizu, T., Sanoh, S., Ohta, S., 2018. Comparison of drug metabolism and its related hepatotoxic effects in HepaRG, cryopreserved human hepatocytes, and HepG2 cell cultures. Biol. Pharm. Bull. 41, 722–732. https://doi.org/10.1248/bpb.b17-00913.
Yu, Y., 2016. Photolysis characteristics of tolfenpyrad in water. Modcrn Agriculture 19, 4–9.
Yuan, Y., Li, X., Wang, J., Feng, Y., Huang, C., Li, Y., Ding, Q., 2017. Degradation characteristics of tolfenpyrad in soil. Agrochemicals 56. https://doi.org/10.16820/j.cnki.1006-0413.2017.02.015 (129-130+137).
Zabel, R., Weber, G., 2015. Comparative study of the oxidation behavior of sulfur-containing amino acids and glutathione by electrochemistry-mass spectrometry in the presence and absence of cisplatin. Anal. Bioanal. Chem. 408, 1237–1247. https://doi.org/10.1007/s00216-015-9233-x.
Zhang, C.-X., Wang, Z.-J., Li, J.-J., Wang, N.-M., Xue, C.-B., 2022. Sublethal effects of tolfenpyrad on the development, reproduction, and predatory ability of Chrysoperla sinica. Ecotoxicol. Environ. Saf. 236, 113482 https://doi.org/10.1016/j.ecoenv.2022.113482.
Zhang, C.-Y., Flor, S., Ruiz, P., Dhakal, R., Hu, X., Teesch, L.M., Ludewig, G., Lehmler, H.-J., 2020. 3,3′-Dichlorobiphenyl is metabolized to a complex mixture of oxidative metabolites, including novel Methoxylated metabolites, by HepG2 cells. Environ. Sci. Technol. 54, 12345–12357. https://doi.org/10.1021/acs.est.0c03476.